Defect Control via Forecasting of Processes' Deviation as JIDOKA Methodology

Dr: Ahmed M. Abed [(1)]and Dr: Adel Abd Elmo'z Ibrahim
Department of Industrial Engineering, Zagazig University, Egypt

Abstract

This paper aims to provide an approach to JIDOKA (machine's autonomation) implementation via compute the proficiency value that based on processes' deviation monitoring to besiege any defects chance weaken competitiveness. The product produced after operating multi-surface spaces (OSS), which prone to deviation during its processes and may lead to defect. The proposed methodology interested in controlling processes' deviation via improving the spatiotemporal model with SARIMA via using 72 observations to study and predict the deviation's behavior to stop machine before defect appears (i.e., JIDOKA methodology). A case study of the manufacture of a lawn mower (carburetor's valve) *is presented to explain the JIDOKA methodology results that demonstrate it accurately and effectively, whether in forecasting or defect suppression to face the* evaporative emissions. *The approach is guided by a six-sigma methodology to obtain improved proficiency. The model's fitting and forecasting results are compared with the SES to prove the ability of applying JIDOKA. The proposed methodology implemented in one of the lawn mower Co. Egypt, which gain defect reduction by 0.7 % or rescue 7000 product every one million via SARIMA(1,1,1)x(0,1,1)$_6$ to improve the spatiotemporal methodology.*

***Key words**: JIDOKA, Machine controlling, ARIMA model, deviation forecasting*

1. Introduction

Egypt participated in the climate conference with the aim of providing industrial solutions to reduce the problem of global warming. The political will decided that the beginning was to control the quality of products that might cause the problem via its evaporative emissions to reduce the pollutants. This agreed by the industrial engineering goal in proposing means of quality control to achieve this goal. The evaporative emissions of a volatile fuel reduced via controlling in carburetor's valve actuation device, which prohibited the fuel flow in its paths, prelude to drained during engine shutdown [8, 18]. Therein lays the importance of manufacturing this valve with minimum deviation or errors. Since the end of the 19th century, the evaporative emissions is in top of manufacturing agenda to reduce the global warming phenomena, which caused via manufacturing a bad carburetor valves in its compressor [24]. Therefore, the design of these valves have subordinated to continuous improvement methodology [22] to emissions suppression to become no-contaminant. The higher proficiency is related with designs that have minimum deviations, which calls for develop and accurate prediction methodologies. The evaporative emissions influenced by valve's unit of compressor shown in Figure-1, which may be divided to three units, the motor, piston/cylinder unit and valve unit, which concerned for verifying the proposed prediction manufacturing methodology. It is extremely difficult to develop a zero defect in manufacturing process in a high-volume environment, which has many manufacturing processes for each part. The continuous monitoring is a viable option via ability to predict how a part manufactured [3]. The spatiotemporal monitoring procedures [2] aided with ARIMA will improve the production planning [20], fault finding and improve proficiency. The processes' capability index is a common standard parameter illustrates the quality level, but it's not sufficient in human intervenes [1]. Therefore, the proficiency index is suggested to measure the efficiency plus effectiveness of the machines and laborers together. The deviation measurement is done after finish every step in the studied process's and hope for do that during process progresses in the future without stopping.

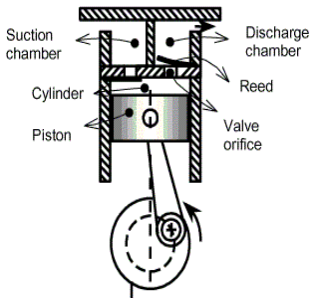

Fig.1: The side view section of lawn mower compressor

The lawn mower compressor as illustrated in Figure-1 consist of a piston moving back and forth in a cylinder, with suction and discharge valves and cause evaporative emissions in failure function [18] due to a bad manufacturing especially in holes radius or thickness dimensions. The suction and discharge valves open and close due to pressure differences between the cylinder and inlet or outlet manifolds respectively. Proficiency is important issue in top agenda of manufacturing process for quality improvement. Because it concerned with main objective, which is producing good product from first time and every time that may be difficult and costly without machine's autonomation approach. While jerky demands (i.e., small different orders) become marketing features [10]. Every stage of products' operation is confronted with numerous errors happening every time [11] and this has brought a big trouble for defect suppression. Many new types of defects striving appear in Egyptian corporates via deviation control. So in this way, accurate deviation forecasting is desired. Any product consists of many operating surface spaces (OSS) that based on many sequential processes, (i.e., $product = \sum_{j=1}^{n}(OSS)_j$. each of them $OSS = \sum_{i=1}^{n} process_i$. In this paper presents the autonomation via

1 Corresponding author email: idealstandarddeviation@gmail.com

fully Bayesian spatiotemporal analysis [24] (i.e., monitors a relative risk surface using a Gaussian Process formulation) for count deviations occur during product produced taking into account the inclusion of an OSS/time interaction term. ARIMA (created by George E.P.Box and Gwilym M.Jenkins in 1970) [7] used 72 observations to fitting this deviation to create effective machine controlling in specific stage and time (JIDOKA). This relative risk surface is used as the mean in Poisson likelihood for the observed counts of deviation (error) by machine. Creating effective JIDOKA using hybrid time series and spatiotemporal analysis model to make short-term forecasting of deviation [5, 6] is a new research field appearing recently. The spatiotemporal proposed by Adelson and Bergen (1985) has become the standard reference model for low-level, Fourier-based deviation sensing in the human visual system. The model is also elegant in its simplicity, and straightforward to implement in about 56 lines of Matlab code. The model is so easy to apply to any 1-D deviation stimulus that I believe the first step in seeking to explain any low-level deviation phenomenon should be to apply the model. The image of operating steps of product can be plotted in a three-dimensional which has two spatial dimensions (x and y) and a temporal dimension (t). A two-dimensional cross-section through this volume along a fixed y-axis produces an x-t plot; x-position as a function of time. Movement creates oriented structure in x-t space, known as spatiotemporal orientation. The angle of tilt corresponds to the velocity of deviation.

The deviation's monitoring is probabilistic problem characterized by uncertainty in all of parameters forecasts. Therefore, the competitors for this method are univariate time series (e.g., dependence and variation through our relative risk surface) or heat maps [4] (e.g., enables temporal forecasts, with uncertainty intervals). The proposed model outperforms current models, because it could be used to answer questions like, how much did deviation (error) distributed over the operating surface spaces [6], and was this normal or not?

The proposed model results will be compared with the simple exponential smoothing (SES) as illustrates later in Figure-24. The paper is organized as following: firstly, the principles of spatiotemporal formulation, the former phase of proposed methodology, the second phase of proposed methodology using ARIMA, the formulation of ARIMA model based on defect data.

2. Manufacturing environment of lawn mower compressors

The experimental study can be divided into; 1) the valve plate that control in evaporative emissions stability and 2) The rotary valve [9]. The samples picked from the same production lot in different weeks with same geometrical parameters. The analysis herewith corresponds to a domestic lawn mower of a cylinder capacity 6.64 cm, working with R134a and a nominal frequency of 50 Hz. Suction, compression and discharge processes are the main processes of compressor in lawn mower, which are executed through valve plate orifices and discharge orifices. Consequently, this paper aims to guarantee the quality of parts in lawn mower performance that causes evaporative emissions, if produced in a bad case.

2.1. Experimental Design

The experiments are focused on valve unit, which including valve plat, valve gaskets, cylinder head and muffler. The selected control factors for valve unit are valve thickness (V_{th}; 2.75: 2.85 *mm*), discharge orifice radius of valve plate (R_{vp}; 2.88: 3.120 *mm*) and discharge orifice radius of crank case (R_{cc}; 2.275: 2.525 *mm*) of tolerance limit as illustrated in Figure-2 and 3. The experiments are executed according to half factorial method in 2 trails (3 factors in 2 levels). During experiments, half factorial designs were used to study the effects of all the factors on the final evaporative emissions responses. The experiment handled the data of 24 lawn mower are collected based on eight samples of data of a two-level DOE 2^k with 3 replicate. All the samples are manufactured and tested in real manufacturing environment maintaining of rest parameters of other parts. Figure-4 illustrate the significant factors should be controlled during valve plate or crankcase manufacturing to besiege the evaporative emissions and limit from global warming phenomena. Figure-5 advices to control the valve thickness in 2.80 *mm*, discharge orifice of valve plate radius at 2.88 *mm*, whereas the discharge orifice of crankcase is 2.525 *mm* to besiege and prevent the evaporative emissions (all these value with tolerance in μm). The drilling operation is based on four factors; the first is the cutting speed that measured by rpm, which recommends slowness of cutting speed due to rigidity of the setup and the quality of finish. Therefore, the rpm depends on $CS_{(m)}x320/D_{(mm)}$ (CS; Recommended cutting speed in surface meter per minute and D; the diameter of the drill in millimeters), in this case, a15-mm twist drill is to cut medium-carbon steel, with a recommended cutting speed of 21.4 *mpm*, then need 457 : 459 rpm. The second is the feed rate which depends on the depth of cut [8 mm: 12 mm], and the last is the thickness of work piece. The Pareto shown in Figure-4-1 illustrates that deviation in μm depends on cutting speed intersects with feed and thickness.

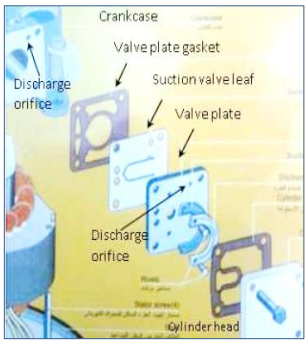

Fig.2: Schematic valve unit of compressor

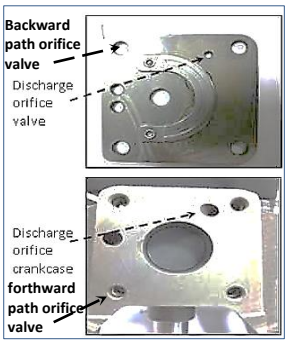

Fig.3: Discharge orifice of valve plate and crankcase

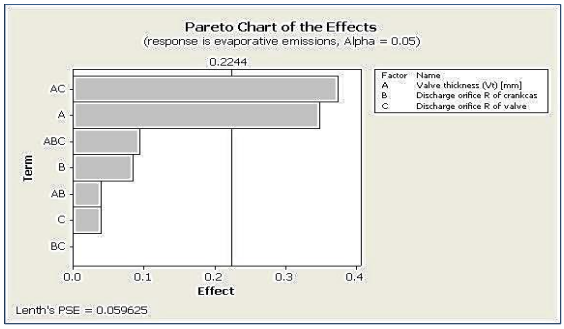

Fig.4: The significant factors causes the evaporative emissions

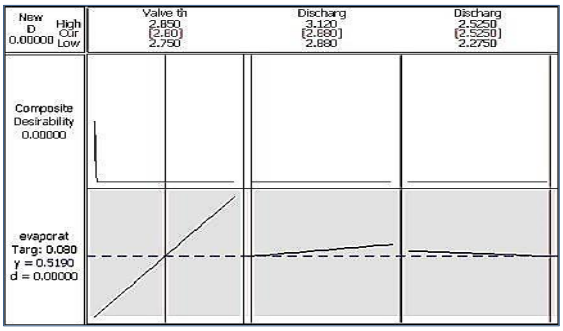

Fig.5: The recommended values of significant factors that prevent the evaporative emissions

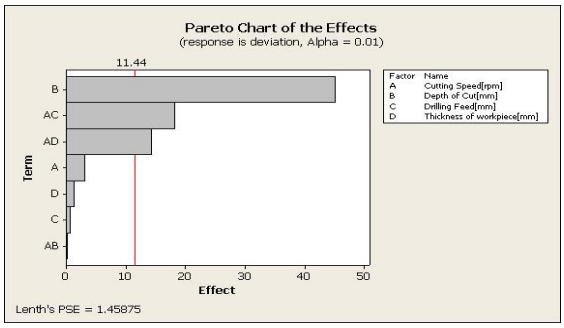

Fig.4-1: The significant factors causes the process deviation

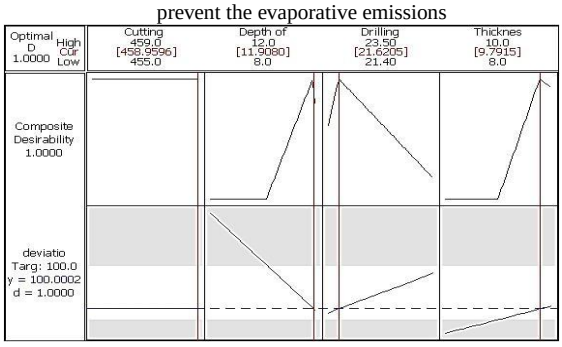

Fig.5-1: The recommended values of significant factors that besiege the deviation

The question is, how can besiege and prevent the evaporative emissions, the answer is, via monitoring the manufacturing processes with time for every significant factor shown in Figure-4. This paper proposed monitoring procedures via spatiotemporal steps which depends on forecasted values fitted via SARIMA model.

3. Proposed Spatio-Temporal ARIMA Methodology [STAM] Formulation

In this paper divides the operating surface space (OSS) of product into matrix of locations as grids. The proposed methodology consists of two phases, the former aims to measure the deviation in different locations on the OSS via six spatio-temporal sequential steps. The second phase predicts the deviation effects' limits (in μm) that fed from the former phase measured via SARIMA, then backward to feed the dataset in the former phase, and so on. The former phase begins with non-oriented test before spatiotemporally test [12]. The data collected should be normalized via convoluted and squared | logarithmic to test its effect with time deviation. The parameters shared in appearing defects as illustrated in Figure-6 during implementing the first phase are (operating surface space area, deviation limits, and number of operating surface space). The intersection between the number of operating surface space and its area ranked high significant, especially with deviation tolerance as illustrated in Figure-6. The dataset consists of spatial data for OSS as illustrated in The proposed system STAM works in functional cycle as illustrated in "Figure 6-1" and is defined in "Table-1"; that are Spatio determination stage, Temporal setting stage, Evaluation stage, ARIMA stage and JIDOKA action stage. A local dataset used in each phase is related to a central database accessed by all running processes. "Figure 6-1" illustrates The STAM conceptual structure; “Table 2” illustrates the role and definition of each part in the system. Figure-7, and temporal data references of deviation values σ_s (deviation span), aggregated by tested machine computed via the activities' uptime $A_{sk}(t)$, which record some of the statistical frequency [17] of deviation appeared at each location s lead to defect, if neglect the significant factors illustrated in Figure 4-1. The σ_s caused by the fault events (i.e., the deviation is considered as mirror for malfunction of forth and backward movements) and $\boldsymbol{k}$ express the span of deviation at this location, which have maximum probability to deviation appeared. Whereas, the number of surfaces is related with the deviation appears in these activities cycle time d_s. The deviation effect on the activities' uptime $A_{sk}(t)$ and directly looted effort without any VA. A^0_{sk} represents the σ_s appeared from predecessor step in the same process.

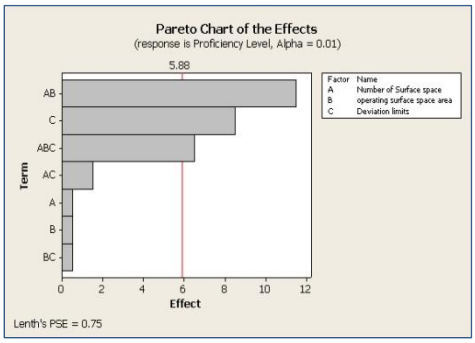

Fig. 6: Pareto chart of spatiotemporal parameters

$$\boldsymbol{A_{sk}(t) = A^{0}_{sk} + d_s(t + \delta t)} \ldots (\mathbf{1})$$

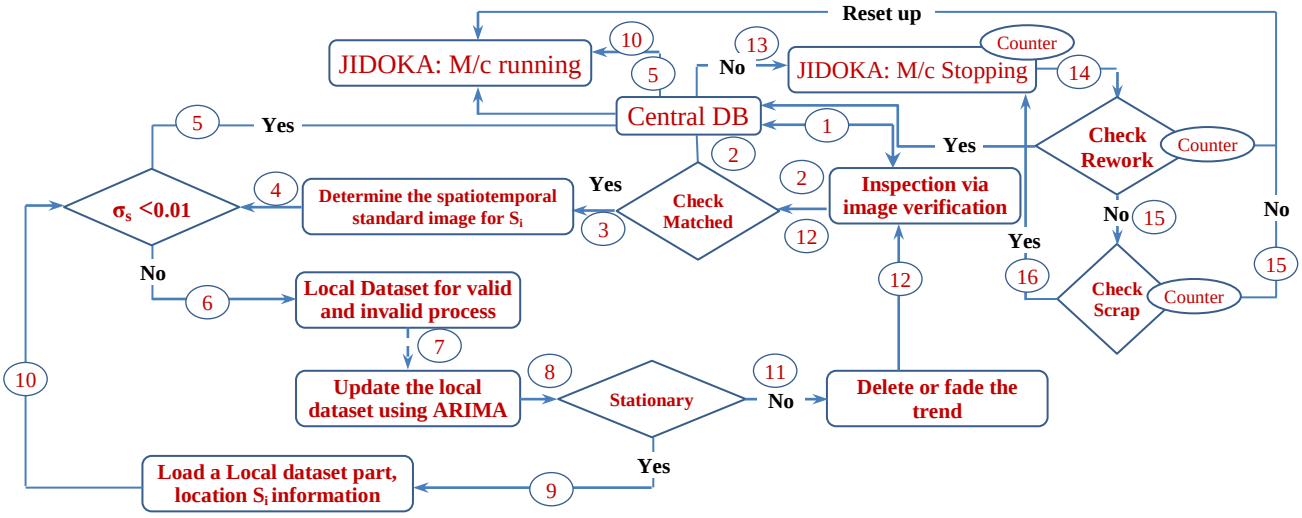

Fig.6-1: The STAM conceptual framework

Table 1. STAM (JIDOKA) cycling functions

NO.	Action	NO.	Action
1	**Select** the part's locations s_i and determine the grid size and measuring specific dimensions	11	Check stationary of saved data in local dataset
2	Insert valid spatio location s_i that have high significant function in specific process in local dataset (review Figure 6)	12	**Delete** or fade the trend in the saved data prelude to forecasting stage
3	Feed the database by the image verification analysis (compared with standard spatio-temporal image) for location s_i.	13	Send forecasted σ_s in μm for STAM methodology in central dataset (x_3)
4	Check for deviation span σ_s temporally and send data to local dataset	14	Receive STAM approval if σ_s <0.01 from central dataset
5	**Create** the central dataset for location s_i and its related standard spatiotemporal images	15	JIDOKA action; [Send data of stopping (if σ_s >0.01) or continuo (if σ_s <0.01)] the machine processing information to local dataset
6	Send an information pulse containing locations s_i and deviation distribution information to Evaluation stage	16	Count the machine downtime and fed the dataset
7	Send Query for STAM methodology in central database	17	Count rework cases and evaluate the STAM instability and fed the dataset with process capability
8	**R**eceive STAM approval from central database if the σ_s < 0.01 (process analysis) or not	18	Count Scrap cases and evaluate the STAM instability and fed the dataset with process capability
9	Send data of valid or invalid process to local dataset and save in database	19	Reset up the machine
10	**Update** the central dataset via ARIMA	20	Continuo the JIDOKA cycle

The data represent deviation's span series of 72 observations (σ_s in micrometer; μm) for specific OSS as shown in Table-2 (Location A) as illustrated in Figure-3 and 7, the average deviation is 133.414 μm and the minimum was 90 μm in week (21) part (5) and maximum is 166.3 μm in the week (52) part (6), which increases by 0.73% and deviate about μ by 24.08454 μm (it is lead to defect in the part's function), the acceptable deviation range for the radius is 120.414 μm < d_s < 148.414 μm, these values indicates the non-homogeneity of data collected, but according to student test it represented via normal distribution. The data also collected and analyzed for other locations i (i.e., B, C and D).

Table 2: The deviation distribution in μm through 52 week

weeks / Part #	W_{21}	W_{28}	W_{34}	W_{36}	W_{38}	W_{40}	W_{42}	W_{43}	W_{47}	W_{48}	W_{50}	W_{52}
	σ_s	σ_s	σ_s	σ_s	σ_s	σ_s	σ_s	σ_s	σ_s	σ_s	σ_s	σ_s
1	97.37	95.51	94.24	127.02	143.54	139.78	156.72	149.4	158.95	151.47	161.54	161.92
2	96	95.44	97.43	126.89	134.42	144.22	142.51	151.23	143.57	155.39	145.7	163.52
3	91.97	90.62	117.65	94.39	136.33	141.11	136.22	154.74	141.67	150.95	139.19	155.46
4	94.16	92.07	120.14	92.3	137.8	142.25	142.04	153.79	142.79	156.69	157.6	140
5	90	90.58	120.29	92.46	138.02	124.99	145.1	127.85	144.32	127.48	157.35	124.81
6	93.61	91.39	123.1	94.83	135.95	136.72	143.35	142.45	145.09	144.17	159.85	166.27

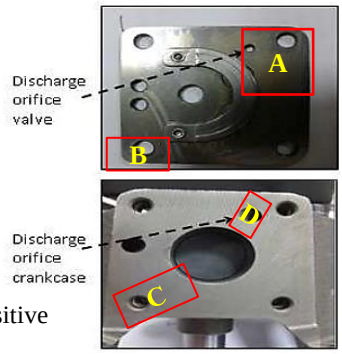

Fig. 7: OSS identification

The operating surface space-time studied regions i = (s, t) as specified in Figure-7 important to covariance calculation and dealing with counted data for specific process in suggested part, which is positive valued (y) and modeled as

$$A_{sk}^{0} = p(y|\lambda) = \frac{\lambda^{y}}{y!} e^{-\lambda} \ldots . (2)$$

The parameter's rate λ (process's progress) varies in space and time λ(s, t) and tackled as positive real-valued function as suggested from Figure 5 and 5-1, so placed a Gaussian Process not on the function itself, but on its log and reformulate as:

$$\boldsymbol{\lambda(s,t) = exp\big(f(s,t)\big) \ldots (2.1)}$$

The proposed methodology considers OSS term σ_s to expect deviation counts at every location s:

$$\boldsymbol{y_{s,t}|\lambda(s,t) \sim Poisson\big(exp\big(f(s,t)\big).\sigma_s\big) \ldots\ldots (2.2)}$$

Eq. (2.2) interprets *exp* (*f* (s, t)) as the relative causes and *f* (s, t) as log-relative causes. If *f* (s, t) turns to 0, *exp*(*f* (s, t)) turns to 1, so $y_{s,t}$ has a Poisson distribution with stationary μ through location s (i.e., σ_s), except that , the exp(*f* (s, t)) >= 1 if f_1 is positive and prove that $y_{s,t}$ follows a Poisson distribution with an elevated μ, whereas the μ reduced in opposite case. Therefore, the relative deviation tackled as independent, so the likelihood factors:

$$\boldsymbol{p(y|f) = \prod_{s,t} Poisson\big(y_{s,t} \,|\, \exp\big(f(s,t)\big).\sigma_s \ldots (3)}$$

Every region on the OSS as illustrated in Figure-2 and Figure-7 treated separately and placing a Gaussian Process prior with μ=0 and covariance K. Therefore, $\boldsymbol{f \sim GP(0,K)}$, should be amalgam the spatial covariance function k_s(s,s') and temporal covariance function k_t(t,t') together.

$$\boldsymbol{K(i,i') = k_s(s,s') + k_t(t,t') \ldots\ldots (4)}$$

Whereas, in seasonal case, a periodic temporal term $k_p(t,t')$ should be included

$$\boldsymbol{k_p(t,t') = ln\left|exp\left(-\frac{2\,sin^2\left(\frac{(t-t')\pi}{52}\right)}{l^2}\right)\right| \ldots\ldots (4.1)}$$

Where the case study lasted 52 weeks, the final covariance structure is interpreted as follows:

$$\boldsymbol{K\big((s,t),(s',t')\big) = k_s(s,s') + k_t(t,t') + k_{st}\big((s,t),(s',t')\big) + k_p(t,t') \ldots\ldots (5)}$$

Where:

$k_s(s,s')$: is a Matern covariance function with ν = 3/2, length-scale l_s and variance σ^2_s.

$k_t(t,t')$: is a squared | logarithmic exponential (Radial Basis Function) covariance function with length-scale l_t and variance σ^2_s

$k_p(t,t')$: is a periodic covariance function with period 52 and parameterization as illustrated in Eq. (5).

$k_{st}\big((s,t),(s',t')\big)$: is a separable space-time covariance function with periodic time component parameterized as k_s . k_p with a single variance σ^2_{st} and separate length-scales for space and time.

The proposed methodology, the Student's t-distribution is used with mean μ= 0, scale σ^2= 1, and degrees of freedom ν = 4 as the prior distribution for each parameter [8]:

$$\boldsymbol{p(x) = \frac{\acute{\Gamma}\left(\frac{v+1}{2}\right)}{\acute{\Gamma}\left(\frac{v}{2}\right)\sqrt{v\pi\sigma^2}}\left(1 + \frac{(x-\mu)^2}{v\sigma^2}\right)^{-(v+1)/2} \ldots\ldots (6)}$$

The results compared between Normal distribution with μ=0 and large variance (one of the traditional choices of "uninformative" or six sigma recommendation [23]) with the Student's t-distribution, which has heavier tails than a Normal distribution. The result proves that it widely useful.

3.1. Phase-1 of STAM

This phase consists of five sequential steps, begins with divided the operation surface space (OSS) into locations (grid scaled from 0 to 100 *mm*) that have maximum deviation as recommended in Figure-4. The phase interests in monitoring the deviation in this locations (i.e., A, B, C or D) during processing time. The following steps simulated via Matlab r2009a.

3.1.1. Non-oriented test [Step 1]

Adelson & Bergen (1985) used spatial functions that were third derivatives of Gaussians [2], which uses a sine wave function windowed by a Gaussian that describes an accurate description of cortical cell receptive fields as illustrated in Figure-8 and set the spatial test profiles with space constant of 0.5 *deg* and spatial frequency of 1.1*cpd*. Whereas, the temporal treated via biphasic; begin with positive response then negative response.

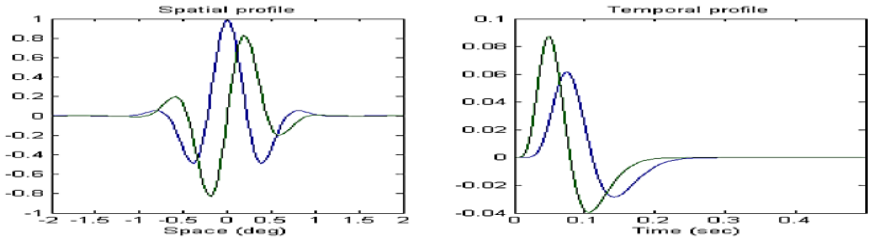

Fig-8: Spatial and temporal profiles

```
% Step 1a ----------------------------------------------------------------------------------------------
%Define the space axis (out of operating contour)
nx=180; %Number of spatial pixel (operating surface space)   | max_x =5;          %Half-width (deg)
dx = (max_x*2)/nx;  %Spatial interval(deg)
x_effect=linspace(-max_x,max_x,nx); % A row vector holding spatial intervals
% Spatial parameters
sx=0.5;   %standard deviation of Gaussian, in deg.           | sf=1.1;  %spatial frequency of carrier, in cpd
% Spatial response profile
gauss=exp(-x_effect.^2/sx.^2);   %Gaussian envelope
even_x=cos(2*pi*sf*x_effect).*gauss;   %Even Gabor           | odd_x=sin(2*pi*sf*x_effect).*gauss;    %Odd Gabor
% Step 1b ----------------------------------------------------------------------------------------------
% Define the time axis (sec)
nt=1000;        % Number of temporal responses               | max_t=0.5;      % Duration of impulse response
dt = max_t/nt;  % Temporal interval (sec)
t_effect=linspace(0,max_t,nt)'; % A column vector holding temporal sampling intervals
% Temporal parameters
k = 100; % Scales the response into time units               | slow_n = 9; % Width of the slow temporal in sec
fast_n = 6; % Width of the fast temporal in sec              | beta =0.9; % Weighting of the -ve phase of the
% Temporal response                                          | temporal response relative to the +ve phase.
slow_t=(k*t_effect).^slow_n .* exp(-k*t_effect).*(1/factorial(slow_n) beta.*((k*t_effect).^2)/factorial(slow_n+2));
fast_t=(k*t_effect).^fast_n .* exp(-k*t_effect).*(1/factorial(fast_n)-beta.*((k*t_effect).^2)/factorial(fast_n+2));
% Step 1c ----------------------------------------------------------------------------------------------
e_slow= slow_t * even_x;                                    | e_fast= fast_t * even_x ;
o_slow = slow_t * odd_x ;                                   | o_fast = fast_t * odd_x ;
% Step 1d ----------------------------------------------------------------------------------------------
back_1=o_fast+e_slow; % L1                                  | back_2=-o_slow+e_fast; % L2
forth_1=-o_fast+e_slow; % R1                                | forth_2=o_slow+e_fast; % R2
```

3.1.2. Spatiotemporally oriented tests [Step 2]

In this step add the 'odd_fast' code to the 'even_slow' code in a backward-selective linear behavior, the test done offline [13]. This step aims to define some basic parameters in x-t space.

```
% Step 2a ----------------------------------------------------------------------------------------------
% SPACE: x_stim is a row vector to hold x-positions of the space.
ARIMA_value_width=4;  %half width in degrees                | x_ARIMA_value=-
                                                            | ARIMA_value_width:dx:round(ARIMA_value_width-dx);
% TIME: t_ARIMA_value is a column vector to hold sampled time intervals of the space
ARIMA_value_dur=1.5;    %total duration in seconds          | t_ARIMA_value=(0:dt:round(ARIMA_value_dur-dt))';
% Step 2b ----------------------------------------------------------------------------------------------
load 'ARIMA.mat';  % Oscillating deviation's span due to ARIMA prediction via (phase-2). Loaded as variable
'ARIMA value'. 'ARIMA value'
% Step 2c ----------------------------------------------------------------------------------------------
% Forthward responses                                       | % Backward responses
  response_forth_1=conv2(ARIMA_value,forth_1,'valid');      | response_back_1=conv2(ARIMA_value,back_1,'valid');
  response_forth_2=conv2(ARIMA_value,forth_2,'valid');      | response_back_2=conv2(ARIMA_value,back_2,'valid');
```

3.1.3. Squaring | logarithmic [Step 3], which fade the general trend

```
% Step 3 ----------------------------------------------------------------------------------------------
response_back_1 = response_back_1.^2;                       | response_back_2 = response_back_2.^2
response_forth_1 = response_forth_1.^2;                     | response_forth_2 = response_forth_2.^2;
```

3.1.4. Normalization test [Step 4]

The next code aims to re-scaled the output to 'normalized' via dividing overall spatiotemporal recorded data by total [15, 21]. The normalization is done via taking the L-R difference (L/(L+R))-(R/(L+R)) = (L-R)/(L+R) as suggested by (Schwartz & Simoncelli, 2001).

```
% Step 4a ----------------------------------------------------------------------------------------------
% Calc back and forth effect
effect_forth= response_forth_1 + response_forth_2;          | effect _back= response_back_1 + response_back_2;
% Calc total effect
      total_effect = sum(sum(effect _forth))+sum(sum(effect _back));
% Normalize
RR1 = sum(sum(response_forth_1))/total_effect;              | RR2 = sum(sum(response_forth_2))/total_effect;
LR1 = sum(sum(response_back_1))/total_effect;               | LR2 = sum(sum(response_back_2))/total_effect;
% Step 4b ----------------------------------------------------------------------------------------------
forth_Total = RR1+RR2;          %predicted via ARIMA        | back_Total = LR1+LR2;          %predicted via ARIMA
```

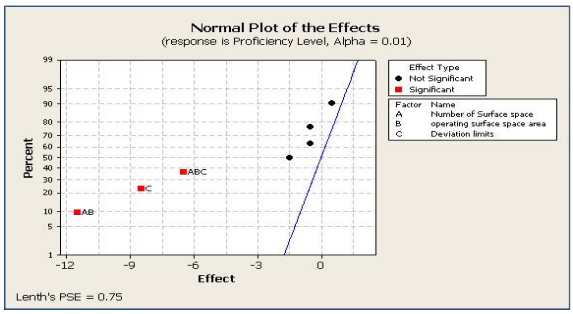

Fig-9: Spatiotemporal parameters Normalize

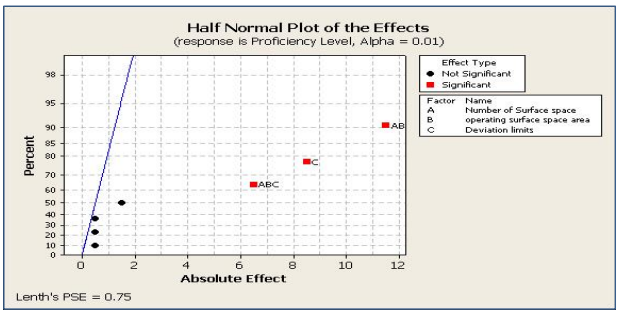

Fig-10: Spatiotemporal parameters Half Normalize

3.1.5. Net deviation effect [Step 5]

Finally, a single score for net deviation effect across the whole x-t image is produced by taking the difference between the two directional scores

```
% Step 5 ------------------------------------------------------------------------------------------------
deviation_effect = forth_Total - back_Total;
fprintf('\n\nNet deviation effect = %g\n\n',deviation_effect);
```

The results collected as illustrated in Figure-11 prove that low deviation appeared in locations (B) and (D), whereas the higher deviation rate appeared in location (A) and may stationary in location (C).

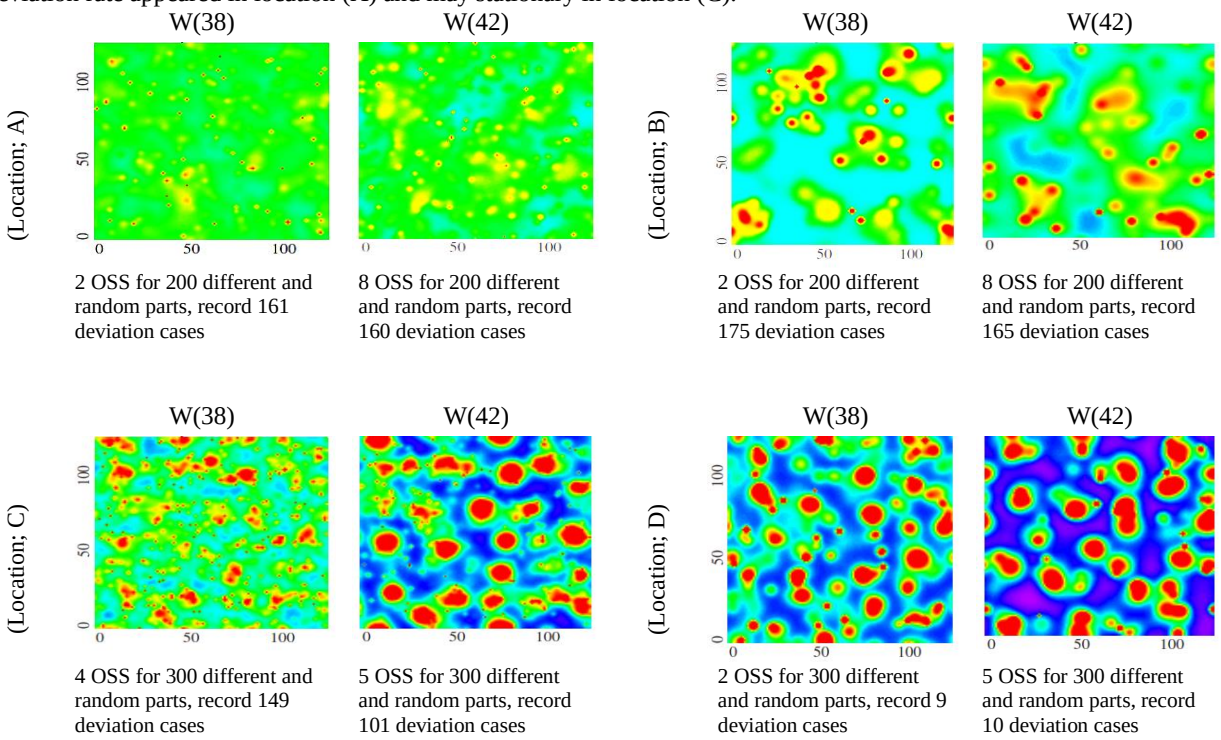

Fig-11: Spatiotemporal results for different locations in OSS

3.2. The second phase of proposed methodology

The 2nd phase intended to benefit from all significant factors effect on manufacturing processes related with evaporative emission in selective product. Graph of data shown in Table-1 (the tolerance of significant factors in μm) expressed by Eq. (6) defines its primary characteristics of deviation behavior as illustrated in Figure-12, which appear increasing trend with time and many periodic fluctuations between peaks and valleys, which revealed to general and seasonality properties. These data represent the summation of forth-ward and back-ward responses to control the deviation [16].

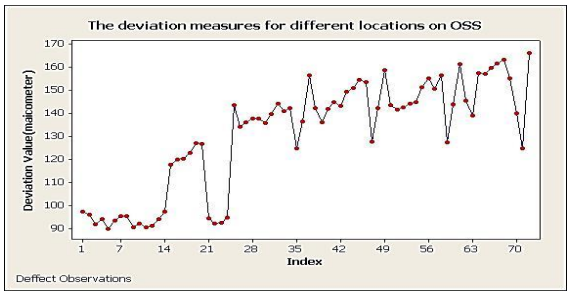

Fig. 12: Primary characteristics of deviation distribution

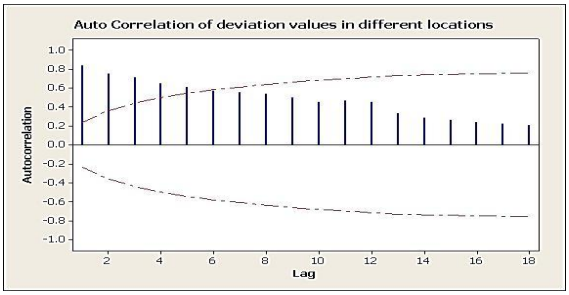

Fig. 13: Autocorrelation of deviation distribution

It is important to extracting the ACF and PACF for the deviation distribution as illustrated in Figure-13 and Figure-14 respectively, that appear the parameters is significant different about zero to spike 18, and it's out of confidence range $-0.215 \leq r_k \leq 0.215$. Therefore, the next step will test the stationary case.

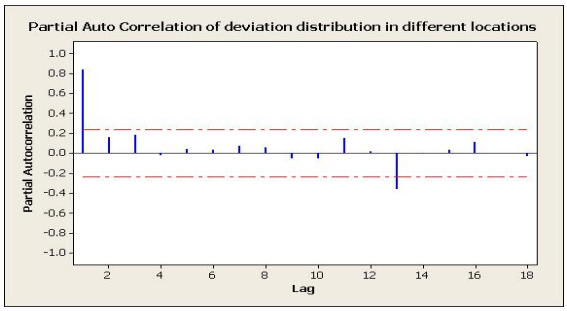

Fig. 14: Partial Autocorrelation of deviation distribution

3.2.1. Stationary test [step 7]

The stationary case test depends on treating the data with logarithmic (ln) as suggested in Eq. (4.1) to fade the general trend as illustrated in Figure-6 and Figure-14 respectively for the deviation distribution. Figure-6 presents close view for our objective for fading the trend. Therefore, based on the logarithmic transformation to choose the suitable SARIMA parameters after extracting these parameters via ACF and PACF, which significantly different about zero till spike (18) and not lay in confidence range $-0.215 \leq r_k \leq 0.215$. **LIung&Box** declares the rejection of the original assumption H_0 because $Q.stat = LBQ\ (TBF) = 383.59 > x^2_{(18,0.01)} = 34.81$, Now refuse $H_0: \rho_1 = \rho_2 = \Delta\Delta = \rho_k = 0$ and belief of no stationary in deviation distribution data.

3.2.1.1. Fade the trend

Select the near distribution (i.e., logarithmic) that reduces the data trend and repeat taking the differences for its value till fade the trend $\nabla Y_{t\ (logarithmic)} = Y_{t(logarithmic)} - Y_{t-1(logarithmic)}$ as illustrated in Figure-15, but must repeat the LBQ test to the first difference $LBQ\ (TBF_{first\ diff}) = 32.52 < x^2_{(17,0.01)} = 33.41$. Therefore, should not take the second difference for the TBF data and accept H_0. Which should in parallel to the axis of the joints, to prove the absence of the general trend as illustrated in (Figure-16) Then preferable [d=1], but (Figure-15 and Figure-16) illustrate the seasonality behavior for the birth-time factor for the location span at spike 12.

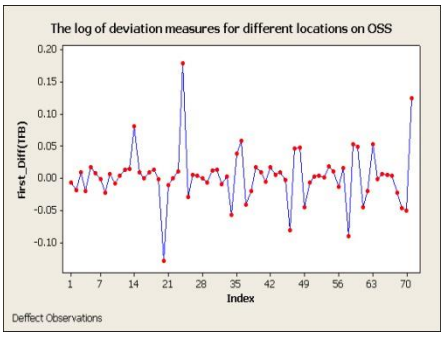

Fig. 15: Absence of trend

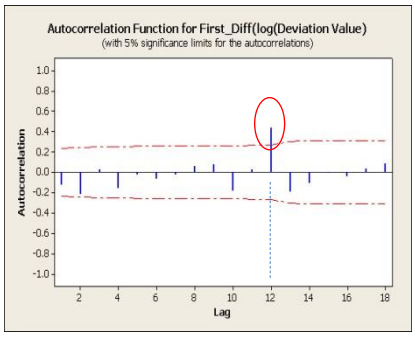

Fig. 16: ACF after first difference

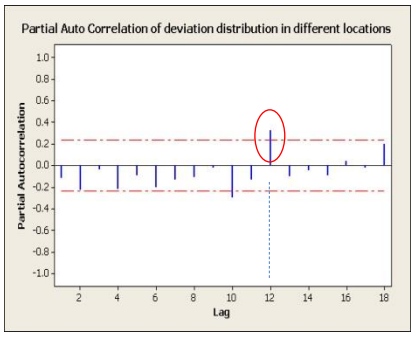

Fig. 17: PACF after first difference

This is accomplished by modifying Eq. (1) to try fading of seasonality attribute and determine the critical location span that has maximum probability of deviation events [14] through time scale ω:

$$\boldsymbol{d_s(t+\delta t) = \left[(1-\vartheta)d_s(t) + \frac{\vartheta}{z}\sum_{s'\sim s} d_{s'}\,(t)\right](1-\omega\delta t) + \theta E_s(t) \dots\dots (7)}$$

Where z, the number of steps planned to be executed on location s, and ϑ is simply a binary parameter between zero and unity that measures the significance of stage affected (i.e., keep average activity cycle time as planned or not). Higher values of ϑ increasing the deviation and lead to a greater degree of defect occur, and lower values lead to the opposite. Equation (7) can be rewritten as Eq. (7.1) to fade any general trend in Fault behavior.

$$\boldsymbol{d_s(t+\delta t) = ln\left[(1-\vartheta)d_s(t) + \frac{\vartheta^2}{z}\sum_{s'\sim s} \Delta d_{s'}\,(t)\right](1-\omega\delta t) + \theta E_s(t) \dots\dots (7.1)}$$

$$\Delta \boldsymbol{d_s(t)} = \frac{\left(\sum_{s' \sim s} \Delta \boldsymbol{d_{s'}}\,(\boldsymbol{t}) - \boldsymbol{z d_s(t)}\right)}{\boldsymbol{\gamma^2}} \ldots\ldots (\mathbf{7.1.1})$$

Where Δ is the discrete Laplacian operator and γ is the average activity's cycle time (in minute) for specific process at location *s*. take the difference for 6 lag to fade the trend as illustrated in (Figure-18)

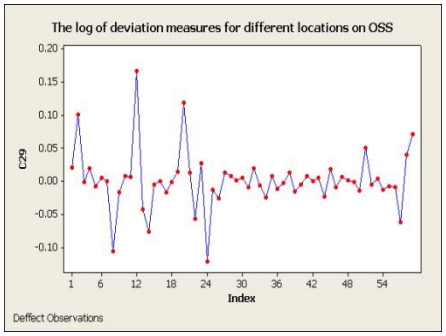

Fig. 18: Absence of trend

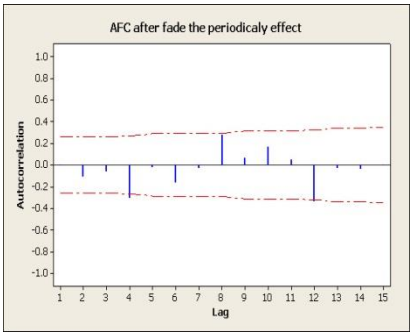

Fig. 19: ACF seasonality first difference

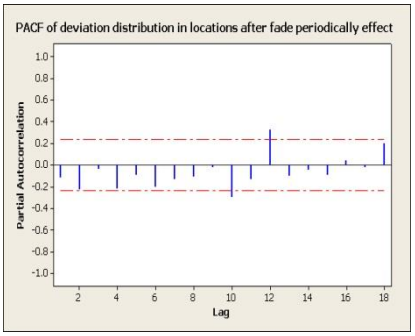

Fig. 20: PACF seasonality first difference

$LBQ\ (TBF_{first\ seasonality\ diff}) = 20.62 < x^2{}_{(15,0.01)} = 30.58$. Therefore, accept the assumption H_0 for seasonality case.

All stages have the same locations' activities $\bar{A}$, and, on average, the same number of steps $\bar{n}$ for the locations of any stage to stay constant, the value by which the location time decays in one time-step $\boldsymbol{\delta t}$ should be equal to the value by which it increases due to fault actions. Similarly, in order for the number of faults at a stage to remain fixed, the number of steps alerted in one timestep (equal to the number of fault events during that timestep) must be equal to the number of steps produced at that stage at rate $\boldsymbol{r_{ijk}}$:

$$\boldsymbol{\bar{n}\,\bar{p}\,\beta = \omega \bar{F} \delta t = r_{ijk} \delta t} \ldots\ldots (\mathbf{8})$$

The derivation of continuum limit by analyzing the dynamics of $F_s(t)$ behavior in greater detail expresses the expected value of the dynamic locations and faults after one timestep as

$$\boldsymbol{d_S(t+\delta t) = ln\left[d_s(t) + \frac{\vartheta \gamma^2}{z} \Delta d_s(t)\right](1 - \omega \delta t) + \beta n_s(t) p_s(t)} \ldots . (\mathbf{9})$$

The $n_s(t)$ is the number of steps that changed according to stage with time, and multiplied by γ^2 to renaming $\rho\ (x,t)$ constant (probability of deviation appearing in determinant location span). Then if subtract $d_s(t)$ from both sides of the equation and then divide the equation by δt. Finally, take the limit as both δt and γ become small, with the constraints that the ratio $\gamma^2/\delta t$ remain fixed with a value define as W (i.e., expected location is all steps executed at every stage including all fault events), and the quantity $\beta\delta t$ also remain fixed with a value ε. The resulting equation gives the dynamics of the locations. The faults propagate throughout the locations while simultaneously decaying in time and reacting with the laborers to create even more locations. Laborers are depleted (i.e., inactive) through reactions with faults and are found themselves execute it at a constant rate. Therefore, if we integrate the stationary of Eq. (9) over entire stages, the averaged fault rate density is matched with γ, assuming that the faults propagation are either zero or is periodic (seasonality).

$$\bar{F} = \frac{\varepsilon W \gamma}{\omega} \ldots (10)[23]$$

The natural time scale for proposed regime is given by $\tau \equiv 1/\omega$, as discussed previously. A characteristic time scale can be defined as $\gamma \equiv \sqrt{\frac{W}{\omega}}$…… (10.1)

$$\boldsymbol{\bar{A} = A^0 + \bar{F}\ and\ \bar{\rho} = \frac{\bar{F}}{A^0 + \bar{F}}} \ldots\ldots (\mathbf{10.2})$$

If the AFC spreads down toward zero by power sequence, then the rank of (p) determined through number of AFC which different about zero. While, if the PAFC down toward zero by power sequence, then the rank of (q) determined through number of statistical correlation (MA). Figure-21 illustrates the residual analysis:

```
                ** Convergence criterion not met after 25 iterations **
Final Estimates of Parameters
Type          Coef  SE Coef       T      P
AR    1    -0.1362   0.1649   -0.83  0.414
MA    1     1.0532   0.0097  108.53  0.000
SMA  12     0.9415   0.1383    6.81  0.000
Constant   0.46981  0.01824   25.75  0.000
Differencing: 1 regular, 1 seasonal of order 6, # of observations:  Original series 65,
after differencing 52, Residuals:    SS = 5795.49 (backforecasts excluded), MS = 137.99
DF = 52
Modified Box-Pierce (Ljung-Box) Chi-Square statistic
Lag              6      24      36           48
Chi-Square    12.7     14.6    34.6          *
DF               8           20      32     *
P-Value      0.124           0.801   0.347  *
```

$LBQ\left(TBF_{first\ seasonality\ diff}\right) = 12.7 < x^2_{(12,0.01)} = 26.22$ That proves the non-significance (stochastic) and the model is effective and efficient to predict the deviation value.

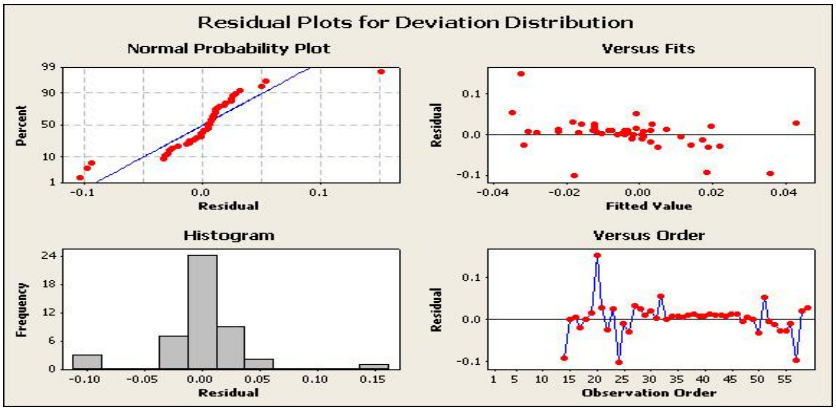

Fig. 21: Residual plots for seasonality deviation behavior

3.2.2. Graphical recommendation output STAM

```
% Plot model output ------------------------------------------------------
% Generate deviation contrast matrix
effect_opponent = effect_forth - effect_back; % L-R difference matrix
[xv yv] = size(effect_back); % Get the size of the response matrix
effect_flicker = total_effect/(xv * yv); % A value for average total effect
% Re-scale ω(normalize) each pixel in the L-R matrix using average effect.
deviation_contrast = effect_opponent/effect_flicker;
% Plot, scaling by max L or R value
mc_max = max(max(deviation_contrast));
mc_min = min(min(deviation_contrast));
if (abs(mc_max) > abs(mc_min))
    peak = abs(mc_max);
else
    peak = abs(mc_min);
end
figure
imagesc(deviation_contrast);
colormap(gray);
axis off
caxis([-peak peak]);
axis equal
title('Normalised spatiotemporal Effect');
%--------------------------------------------------------------------------
```

Eq. 10.3 and Eq. 10.4 used to determine the critical location span that besieges the maximum deviation probability as illustrated in (Fig.15)

$$\boldsymbol{A(X,t) = \bar{A} + \delta A^{e^{\sigma t} e^{i\phi.x}}} \ldots\ldots (\mathbf{10.3}) \qquad \boldsymbol{\rho(X,t) = \bar{\rho} + \delta \rho^{e^{\sigma t} e^{i\phi.x}}} \ldots\ldots (\mathbf{10.4})$$

The deviation done due to intervening the human and physical resources at any given step affected by a seasonal index Ø]1: ∞[(which treated by setting the autoregressive rank in prediction regime) for every A and ρ for any fault type at any stage via the following matrix:

$$\begin{bmatrix} -\vartheta|\emptyset|^2 - 1 + \bar{\rho} & -\bar{A} \\ \frac{2\bar{\rho}}{\bar{A}}|\emptyset|^2 - \bar{\rho} & -|\emptyset|^2 - \bar{A} \end{bmatrix} \begin{bmatrix} \delta_A \\ \delta_\rho \end{bmatrix} = \sigma \begin{bmatrix} \delta_A \\ \delta_\rho \end{bmatrix} \dots\dots (11)$$

When representing the matrix (11 via Matlab to find σ. Linear instability is present for all values of deviation σ that are greater than zero as illustrated in Figure 22, which will appear at seasonal index Ø for which the determinant of the coefficient matrix in Eq. (11) is negative. Then make sure that the proficiency affected with the deviation span and its lifetime, which affected by seasonal index Ø.

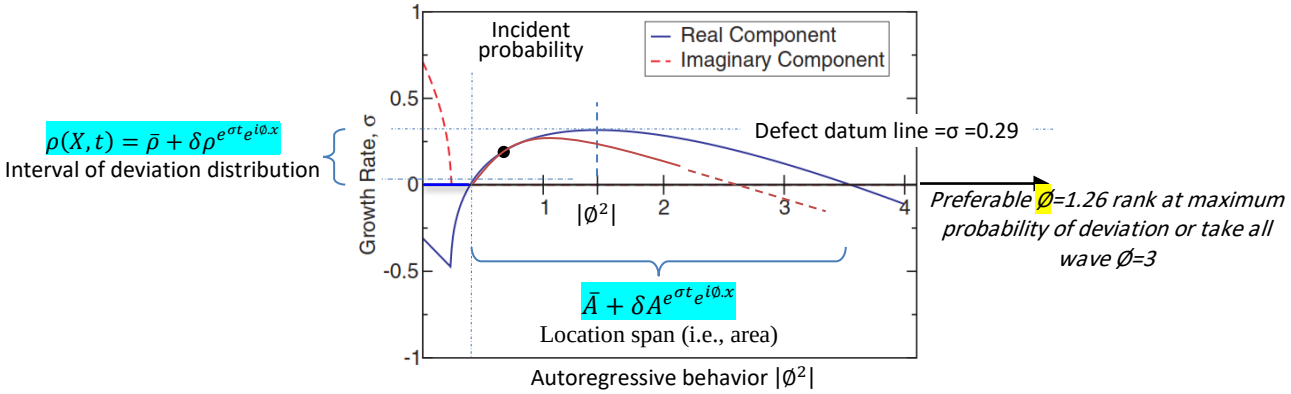

Fig.22. Solving Eq. (11) represents the growth rate **σ** for a linearly unstable process in decreasing rate, then decay (i.e., location area) and repeated every step. The imaginary component is nonzero over planned for which the real component is negative, indicating no growing oscillations in the process. The real component is positive over a finite band of planned, and has a peak at a value |Ø ²|; this maximally growing behavior should set the final size of high deviation that may lead to defect.

If the proposed methodology detects instability in the process, there will be seasonality Øw that exhibits the fastest growth rate of all unstable behaviors. This maximally growing behavior can be shown to be given by

$$|\emptyset_w|^2 = \frac{\mathbf{1}-\bar{A}}{\mathbf{1}-\vartheta} - \frac{\bar{\rho}(5-\vartheta)}{(1-\vartheta)^2} + \sqrt{\vartheta(1+\vartheta)^2\bar{\rho}[(\bar{A}(3-\vartheta)-2)(1-\vartheta)+2\bar{\rho}(3-\vartheta)}\frac{1}{\vartheta(1-\vartheta)^2} \dots . (13)$$

Box-Jenkins informs that estimating the residual et (α_t is the white noise factor, when the residual normally distributed in constant μ and σ^2 which differ significantly from zero. (If it is not significant, then exclude some of AR, MA ranks)) to test independency and randomly of residual by the next formula:

$$P_r\left\{-2.576\left[\frac{1}{\sqrt{n}}\right] \le P_k(\alpha_t) \le +2.576\left[\frac{1}{\sqrt{n}}\right]\right\} = 0.99$$

$$\text{In this step } Q = T(T+2)\sum_{k-1}^{k}\frac{1}{T-k}p_k^2 \dots\dots\dots (14)$$

The best decision for the ARIMA model which achieve p-value < 0.01 for MA(q), otherwise is refused. Therefore, the regime should predict the fault's birth-time and its expected lifetime on time, taking into account the preferable moving average value $|\emptyset|^2 = 1.6$ and $\emptyset = 1.2649$ to besiege instability appears at $\sigma_{max} \geq$ [0: 0.29] for birth-time late, because their effects on proficiency will be crucial. ARIMA is suggested to this phase and adjust the MA (Ø=1.2 at maximum probability or 3 for all wave band). The preferable model SARIMA (1, 1, 1) x (0, 1, 1)$_6$ is efficient and effective. Therefore, X_t (significant factors) and the residual e_t to get the future forecasting value for X_{t+1} (forth-ward response) and use forecasting value as present to the next X_{t+2} (back-ward response). If the tolerance greater than 160μm, will refused and considered scrap, whereas if it less than 140μm considered reworked. The spatiotemporal scanning will run at period 73, 80 and 83 for studied product as illustrated in Figure-23.

$$\boldsymbol{ex-post}: X_{t+1} = B_0 + \emptyset X_t + \emptyset_1 X_{t-1} + \sigma_t - \theta_1\sigma_{t-1} \qquad \boldsymbol{ex-ante}: X_{t+2} = B_0 + \emptyset_1 X_{t+1} + \sigma_t - \theta_2\sigma X_t$$

Forecasts the deviation distribution from period 72 [99% Limits (location span]

Period	Forecast	Lower	Upper	Period	Forecast	Lower	Upper
73	175.484	157.650	193.318	79	159.317	135.986	182.649
74	158.606	137.880	179.331	80	160.406	136.843	183.968
75	154.242	132.400	176.084	81	152.119	128.336	175.901

76	158.009	135.592	180.427	82	148.893	124.896	172.890
77	156.718	133.926	179.509	83	130.424	106.217	154.632
78	156.297	133.215	179.378	84	147.070	122.655	171.485

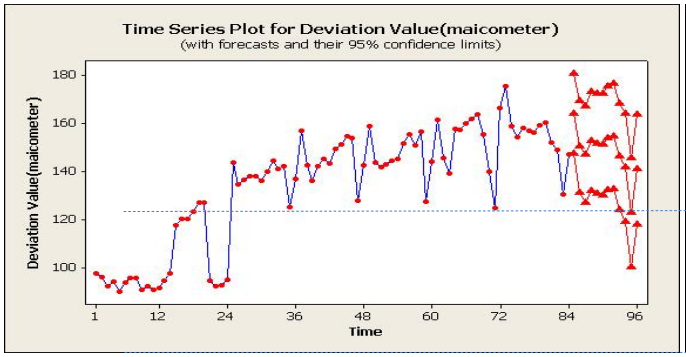

Fig. 23: The Prediction phase for the deviation distribution

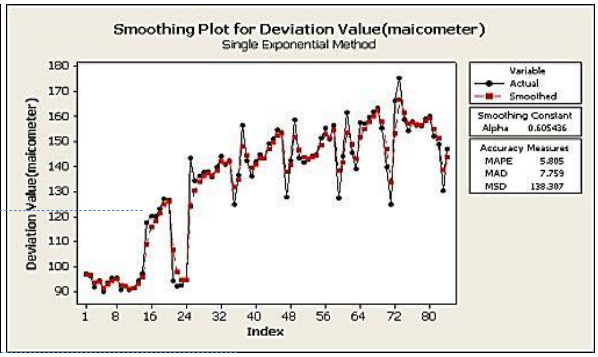

Fig. 24: The comparison between proposed STAM and SES for deviation distribution

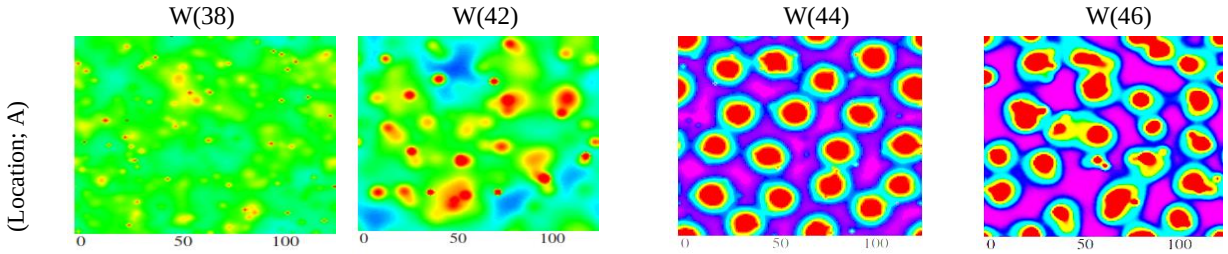

3 OSS for 311 different and random parts, record 157 deviation cases

5 OSS for 311 different and random parts, record 72 deviation cases

9 OSS for 311 different and random parts, record 15 deviation in rework cases

9 OSS for 311 different and random parts, record 9 deviation in rework cases

Fig-25: Spatiotemporal results for locations (A)

Figure-26 motivate to reduce the number of operating surfaces to 5 or less if the operating surface span fitted between 10 *mm* and 13 *mm*, or between 20 *mm* and 24 *mm*. The optimal output obtained when the operating surface span set at 12 *mm* and the number of operating surfaces at 9, in this case the deviation will be less than 0.1 and the evaporative emissions will suppression. Therefore, re-run the proposed STAM code, and set the number of operating surface between 3, 5 and 9 and activate the ARIMA to predict with the deviation in time to stopping the machine and rescue the product.

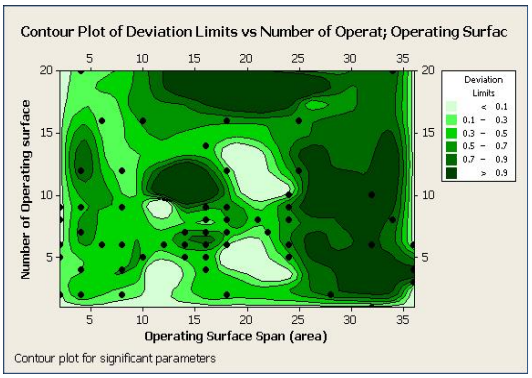

Fig. 26: The recommendation of spatiotemporal aided with ARIMA to reduce deviation

4. Conclusion

In this paper, time series model of SARIMA is used to make short-term forecasting of deviation behavior aided for spatiotemporal for selected part in specific product share in global warming phenomena in Egypt. The fitting and forecasting results are compared with the other forecasting tool (SES) as illustrated in Figure-24. The result shows that STAM fits the data well and makes higher accurate forecasting than the other model. This work is proved to be very helpful to the quality department in improving the efficiency of decision-making and emergency management. This paper presented a general framework for the statistical modeling of spatiotemporal count data. There is nothing special about deviation events, and early experiments using our methods to forecast 311 (calls for non-emergency services like potholes) have been promising. In the application of this framework, a series of modeling decisions which would be worth exploring in more detail in future work was made. The use of spatiotemporal leading indicators—other deviation (errors) types, weather patterns, other events measured online or offline—might provide measurable improvements in our forecasts.

Table-3 illustrates the comparison between proposed methodology and recent reported results using SES statistical models [1, 12, and 14] is also needed.

Table-3: The comparative study before and after STAM implementation

	STAM		Improvment	SES
	Before	After		
The Number of high deviated parts and decided as (rework) [ppm]	12000	150	98,75 %	12158
The Number of high deviated parts and reject (scrap) [ppm] review process capability	7000	8	99,89 %	7042
The Number of standard part produced (μ =0.01) [ppm]	621,548	896,245	44,19 %	703,926
The Number of high deviated parts but accept [ppm]	366,212	103,605	71,70 %	118,354
Instability deviation $Ø_w$ for discharge orifice valve	3850	1	~100 %	4129
Instability deviation $Ø_w$ for discharge orifice crankcase	3150	7	~100 %	2913

5. Future work

The proposed framework does incur computational burden done via Matlab r2009a. There is much field for the further development of approximation techniques and new formulations of methodologies for fitting spatiotemporal data online. The proposed framework based entirely on measurements data that collected to compensate for modified Matlab code, should considered in the future as a baseline for comparison.

References

[1] Ahmed M. Abed, (2016). "Adjust Jidoka Occupational Fatigue to Reduce Idle times using Data Mining as Lean Tool".,EIJEST, The Egyptian International Journal of Engineering Science and Technology, Vol (19) No (2). Pp 312- 318.
http://www.eijest.zu.edu.eg/index.php/EIJEST/issue/view/94

[2] Allen, J.C., C.C. Brewster and D.H. Slone, (2001). "Spatially explicit ecological models: a spatial convolution approach". Chaos, Solitons and Fractals, Vol. 12, Pp. 333–347.

[3] C. Cho, D. D. Kim, J. Kim, D. Lim, and S. Cho, (2008). "Early prediction of product performance and yield via technology benchmark," IEEE Custom Intergrated Circuits Conference (CICC), Pp. 205-208.

[4] Feng-Mei Tseng, Gwo-Hshiung Tzeng, (2002). "A fuzzy seasonal ARIMA model for forecasting," Fuzzy Sets and Systems. Vol. 126, Pp. 367-376.

[5] Gorr, W. L., Olligschlaeger, A. M., & Thompson, Y., (2003). "Short-term time series forecasting of deviation,". International Journal of Forecasting. Vol. 19, Pp. 579-594.

[6] George E.P.Box and Gwilym M.Jenkins & Gregory C. Reinsel, (1994). "Time series analysis forecasting and control,". Prentice- Hall, Inc.4.

[7] H.Brian Hwarng, H.T.Ang, (2001). "A simple neural network for ARIMA (p.q) time series,". Omega. Vol. 29, Pp. 319-333.

[8] K. L., Challinor, & Mather, G., (2010). "A motion-energy model predicts the direction discrimination and MAE duration of two-stroke apparent motion at high and low retinal illuminance,". Vision Research, Vol. 50, Iss. 12, Pp. 1109-1116.

[9] Mather, G., & Challinor, K. L., (2009). "Psychophysical properties of two-stroke apparent motion," Journal of Vision, Vol. 9 Iss. (1:28), Pp. 1-6.

[10] M. Sameh Ibrahim, M. A. R. Mansour, A. M. Abed. (Sept-2011). "Improve six-sigma management by forecasting production quantity using image verification quality tool", International journal of advances in engineering and technology (IJAET), ISSN 2231-1963, Vol. 1, Iss. 4, No. 53, Pp 332-342.

[11] Powell, J.A. and N.E. Zimmermann, (2000). "Multi-Scale Analysis of Seed Dispersal and the Resolution of Reid's Paradox," Submitted to Ecology.

[12] Pace, R. Kelley and Ronald Barry, O.W. Gilley, C.F. Sirmans, (April-June 2000). "A Method for Spatial-temporal Forecasting with an Application to Real Estate Prices," International Journal of Forecasting, Volume 16, Number 2, , p. 229-246.

[13] S. Ibrahim, M. Abdel-halim, and A.M. Abed, (2010). "Machine Downtime Reduction By Defect And Labor Control" AL-Azhar Engineering 11th International Conference, AEIC 11, Egypt, December 23-24, and JAUES, Vol.5, No.2, pp 83-92.

[14] S. Ibrahim, M. Abdel-halim Mansour, and Ahmed M. Abed, (Jan. 2011). "Improving processes quality by new Lean Six Sigma methodology for revamping online production lines training" The Egyptian Int. J. of Eng. Sci. and Technology, Vol.14, No. 1, Egypt, January 10-12, pp 611-620.

[15] T. Turunen-Saaresti, P. Roytta, J. Honkatukia, and J. Backman, (2010). "Predicting off-design range and performance of refrigeration cycle with two-stage centrifugal compressor and flash intercooler," international journal of refrigeration, Vol. 33, pp. 1152-1160.

[16] Volkan S. Ediger, Sertac Akar., (2007). "ARIMA forecasting of primary energy demand by fuel in Turkey,". Energy Policy. Vol. 35 pp. 1701-1708.

[17] W. C. Chen, G.-L., Fu, P.-H. Tai, and W.-J. Deng, (2009). "Process parameter optimization for MIMO plastic injection molding via soft computing," Expert Systems with Applications, Vol. 36, pp. 114–122.

[18] W. Ma, S. Fang, B. Su, X. Xue, M. Li.. (2017). "Second-law-based analysis of vapor-compression refrigeration cycles": analytical equations for COP and new insights into features of refrigerants Energy Convers Manage, 138, Pp. 426-434

[19] X. Han, J. Pei, J. Liu, L. Xu., (2013). "Multi-objective building energy consumption prediction and optimization for eco-community planning.", Energy Buildings, Vol (66), Pp. 22-32.

[20] Z. Huang, H. Yu, Z. Peng, M. Zhao., (2015). "Methods and tools for community energy planning: a review Renew Sustain Energy.", Rev,

42, Pp. 1335-1348

[21] Wang Yan. Application of time series. Renmin university of China publisher. 2005.

[22] A. D. Sleeper, Design for Six Sigma Statistics. McGraw-Hill, 2006.

[23] D. C. S. Summers, Six Sigma Basic Tools and Technique. 1st ed Prentice Hall, 2007.

[24] M. P. Groover, Automation production Systems, and Computer Integrated Manufacturing. 3rd ed., Pearson, 2008.

Suggested titles

1. Defect Control via Forecasting of Processes' Deviation as JIDOKA Methodology
2. Process control via spatiotemporal aided with ARIMA forecasting Methodology
3. JIDOKA implementation by spatiotemporal and ARIMA forecasting Model
4. Improve spatiotemporal model via ARIMA to reduce defect as a six-sigma tool